# Planar Air-Filled Terahertz Antenna Array Based on Channelized Coplanar Waveguide Using Hierarchical Silicon Bulk Micromachining

Le Chang, *Student Member, IEEE*, Yue Li, *Senior Member, IEEE*, Zhijun Zhang, *Fellow, IEEE*, Shaodong Wang, and Zhenghe Feng, *Fellow, IEEE*

***Abstract*— A planar air-filled terahertz antenna array based on channelized coplanar waveguide (CCPW) is proposed and fabricated using silicon bulk micromachining technology. Planar air-filled four-unit array composed of two silicon layers is verified at 300 GHz. Periodical field blocking stubs are loaded in the gaps of the CCPW alternatively to break the fringing field symmetry, generating an in-phase radiating aperture. The fabrication technology has two features: first, the silicon dielectrics are completely plated with gold, generating a purely air-filled antenna with high performance and second, the hierarchical micromachining method enables a single silicon layer to be divided into two sublayers, resulting in reduced antenna layers. The numerical result shows a simulated −10 dB impedance bandwidth of 71.1 GHz (25.95%, 238.4–309.5 GHz) and stable fan-shaped beams with broadside gains and radiation efficiencies higher than 10.6 dBi and 87.9%, respectively. Experiment of the fabricated prototype exhibits a bandwidth that totally covers the simulation and stable beams with broadside gains higher than 8.6 dBi. To the best of author's knowledge, this is the first time that a planar air-filled terahertz antenna array is proposed. Moreover, confirmation of the strategy demonstrates the antenna's distinguished suitability to realize antenna-in-package solution.**

***Index Terms*— Antenna-in-package (AiP), channelized coplanar waveguide (CCPW), dry etching, gold plating, hierarchical micromachining, terahertz antennas, wet etching.**

## I. Introduction

TERAHERTZ technology, as a new frontier of electromagnetism, has experienced rapid growth [1]. Terahertz brings great opportunities for many industries, such as ultra-broadband wireless communications [2], detection of weapons and contraband [3], disease diagnostics [4], and especially high-resolution imaging owing to its unique spectral characteristic for different material discriminations [5]. Antennas play a critical rule for wireless systems, and terahertz antennas have been experiencing their growing period [6]–[9], [17]–[32], [34]–[36]. For fabricating antennas with extremely small physical volume, the challenge is to find high-precision and low-cost manufacturing processes.

Authors broadly divide the common terahertz manufacturing processes into two types, i.e., the LTCC and silicon technologies. LTCC, as the mainstream multilayer packaging technology, can integrate planar antennas, passive components, and monolithic microwave integrated circuit (IC) into a single package [6]. Substrate integrated waveguide slot array at 140 GHz [7], radial line slot array and cavity-backed Fresnel zone plate lens at 270 GHz [8], and step-profiled corrugated horn at 300 GHz [6] have been made out using the LTCC process. However, the shrinkage problem may increase the tolerance [9], and the most of the LTCC-based antennas were focused on 60 GHz band [10]. Silicon is superior to the other semiconductor materials, such as GaAs, GaP, and InP, owing to the readily available and cheap raw materials. Besides, silicon-based materials are suitable for bonding. However, as for other materials, the high temperature and high pressure may damage the atomic structures, so they cannot be bonded. As for manufacturing antennas, silicon is the best choice. Silicon bulk micromachining technology shares the same abundant fabrication processes with the IC processing technology, including lithography, various etching, photoresist, chemical deposition, sputtering, and plating processes [11]–[16]. Plenty of terahertz antennas have been realized using silicon bulk micromachining, such as silicon lens [17]–[19], dielectric rod waveguide antennas (GaAs wafer is used here) [20], [21], silicon-on-glass-tapered antennas [22], [23], stacked dielectric resonator meander slot [24], antipodal curvedly tapered slot [25], horns [26]–[29], and other basic antenna types, such as monopole, patch, loop, slot, and Yagi [30]–[32].

Dielectric loss becomes a severe problem especially for frequency so high at terahertz band. Antennas with air medium yield good performance. Several kinds of low-loss dielectric waveguide at terahertz band were introduced in [33]. NASA's jet propulsion laboratory has done extensive research on various purely air-filled submillimeter-wave electronic

Manuscript received June 18, 2017; revised May 20, 2018; accepted July 22, 2018. Date of publication August 1, 2018; date of current version October 4, 2018. This work was supported in part by the National Natural Science Foundation of China under Contract 61525104 and Contract 61771280 and in part by Beijing Natural Science Foundation under Contract 4182029. *(Corresponding author: Zhijun Zhang.)*

L. Chang was with the State Key Laboratory on Microwave and Communications, Tsinghua National Laboratory for Information Science and Technology, Tsinghua University, Beijing 100084, China. He is now with Huawei Device Ltd., Beijing 100095, China.

Y. Li, Z. Zhang, and Z. Feng are with the State Key Laboratory on Microwave and Communications, Tsinghua National Laboratory for Information Science and Technology, Tsinghua University, Beijing 100084, China (e-mail: zjzh@tsinghua.edu.cn).

S. Wang is with the Hebei Semiconductor Research Institute, Shijiazhuang 050000, China.

Color versions of one or more of the figures in this paper are available online at http://ieeexplore.ieee.org.

Digital Object Identifier 10.1109/TAP.2018.2862360

components using silicon micromachining technology, such as rectangular waveguide, filter, hybrid coupler, frequency tripler, amplifier, and mixer [34]–[39]. In all those designs, signals are propagating only in air channels, which significantly reduce dielectric loss. In [35], a circuit of micromachined silicon is sandwiched between two metal cavities to form a horn antenna. This paper's authors have previously explored the micromachined silicon process in millimeter-wave antenna designs. Chang *et al.* [40]–[42] have addressed the issue of fabricating purely air-filled antenna with high-permittivity silicon substrate at 60 GHz for the first time. In this paper, for the first time, a planar air-filled terahertz antenna array has been proposed and fabricated using the silicon bulk micromachining technology. Radiation of the proposed antenna is inspired by breaking the fringing field symmetry of the channelized coplanar waveguide (CCPW), and for implementation, a series of field blocking stubs are loaded in the gaps of the CCPW alternatively. Benefiting from the wet etching process, a single silicon layer can be divided into two sublayers for hierarchical manipulation: after wet etching is adopted to process one of the sublayers, the other can be disposed freely using either wet or dry etching. On the other hand, using a combination of wet etching, dry etching, and gold plating processes, all the surfaces of the silicon dielectrics are fully metallized, so the electromagnetic (EM) wave cannot touch any silicon dielectrics, forming a purely air-filled antenna.

The antenna consists of two silicon layers and each layer is micromachined hierarchically. The top layer contains a radiating window and four radiating slots that are fabricated using wet and dry etching, respectively, while the bottom layer contains an air space and a coupling slot that are both fabricated using wet etching. Finally, the two layers are assembled as a whole using the optical alignment and wafer bonding processes. Compared with our previous design, the silicon substrate used is reduced by one layer [40]. The antenna is center-fed using the standard 300 GHz WR-3 waveguide whose center aligns with that of the coupling slot, and an additional copper spacer acts as a bridge connecting the proposed antenna and feeding waveguide. The planar air-filled terahertz array exhibits high performance: the simulated bandwidth is 71.1 GHz (25.95%, 238.4–309.5 GHz), while the measured one is higher than 117.7 GHz ($>$25.95%, 222.3 to $>$340 GHz); the simulated patterns are fairly stable across the band with the broadside gains and radiation efficiencies ranging from 10.6 to 13.8 dBi and 87.9%–97.8%, respectively. The measured patterns and gains roughly agree with the simulation.

Moreover, the silicon semiconductor that is compatible with IC, in addition to the small footprint of the terahertz antenna, facilitate to antenna-in-package (AiP) solution [43]. AiP that can provide highly integration and packaging degree is the new trend of antenna design. The validity of the design strategy provides the possibility to realize the AiP solutions [42].

## II. Radiation Principle

Schematic of the radiating principle based on air-filled CCPW (ACCPW) is illustrated in Fig. 1 [44], where the left column shows the vector fringing E-fields and the right column shows the layered models. The red arrow lines denote the fields along the $+y$-direction, while the blue arrow lines denote the $-y$-direction. Fig. 1(a) depicts the fringing E-fields of the two end-shorted ACCPW: the fields on one side of the center conductor are phase-reversed with their counterparts on the other side, and the standing wave is resonant underneath. The field strength presents a sinusoidal period manner, and stationary nulls and maximums can be observed. To convert the resonant mode to the radiating mode, the symmetrical field distribution needs to be broken in some way. As illustrated in Fig. 1(b), by loading a series of field blocking stubs, i.e., metallic cuboids, alternatively and periodically around the maximums of these blue E-fields in the two gaps, the blue fields are suppressed, while the red fields with the same phase are left within these naturally generated slots, forming effective radiation at broadside. It is worth noting that the two edge stubs are slightly bigger than the others. In physics, for each unit, it is in fact that a T-shaped open cavity radiates from its open side; for the whole array, it is in fact that a series of T-shaped open cavity is cascaded alternatively and periodically, forming an in-phase radiating aperture. Therefore, these blocking stubs convert the ACCPW into an antenna array. It is important that each blocking stub does not necessarily cover the whole area of the half-period field, as long as it is located around the stationary maximum point. Moreover, the proposed antenna has scalability along one direction.

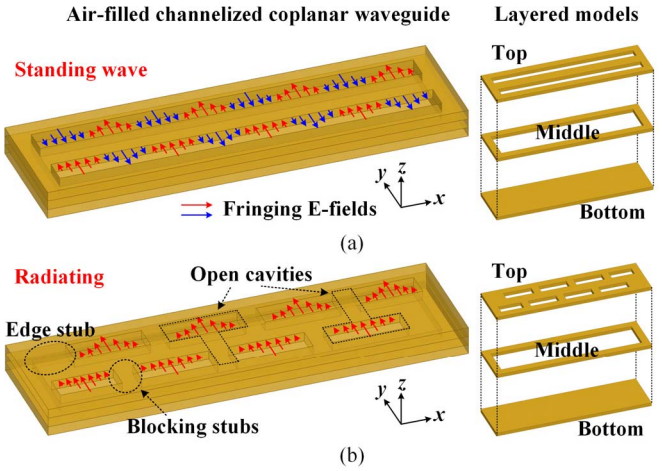


Fig. 1. Schematic of the radiation principle based on ACCPW. (The right column: layered models). (a) Sketch of the vector fringing E-field distribution. (b) By alternatively loading periodical blocking stubs, open cavity cascaded array is constructed, forming an in-phase radiating aperture.

## III. Planar Air-Filled Terahertz Antenna Array

### A. Antenna Configuration

To prove the operating principle, a planar air-filled four-unit terahertz array is taken as an example and analyzed. Configuration of the proposed terahertz array is illustrated in Fig. 2, where (a) shows the perspective view, (b) shows the top view, (c) shows the exploded view of the antenna, (d) depicts the top view of each sublayer, and (e) displays the plane views of the three view angles in (c). The substrate used

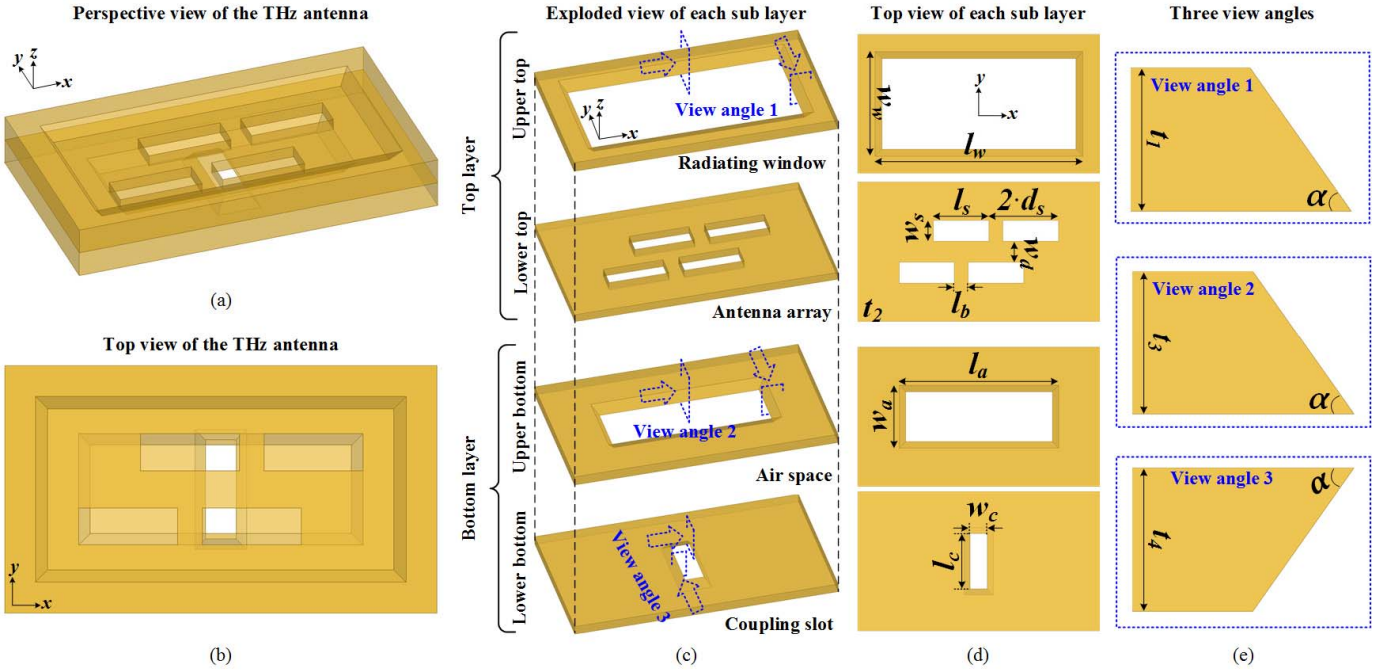


Fig. 2. Configuration of the proposed planar air-filled terahertz antenna array. (a) Perspective view. (b) Top view. (c) Exploded view of the antenna. (d) Top view of each sublayer for dimensions illustration. (e) Plane views of the three view angles in (c).

here is the single-crystal silicon with a thickness of 0.25 mm. The proposed antenna consists of two silicon layers and each layer can be divided into two sublayers for hierarchical fabrication. For the first layer, the upper sublayer with a thickness of 0.14 mm contains a radiating window, and the lower sublayer with a thickness of 0.11 mm contains four radiating slots; for the second layer, the upper sublayer with a thickness of 0.13 mm contains an air space, and the lower sublayer with the thickness of 0.12 mm contains a coupling slot. Among them, the radiating window, air space, and coupling slot are fabricated using wet etching and gold plating processes. The wet etching used is anisotropic etching which produces concave cavities with 54.7° sidewalls as shown in Fig. 2(c) and (e). The four radiating slots are manufactured using dry etching and gold plating processes. The dry etching produces nearly plumbed sidewalls. Alignment relations of the four structures are illustrated in Fig. 2(b): all the structures align with the same body center, and the upper opening of the air space is the smallest rectangular surrounding the four slots. In simulation, the antenna is fed in the center using the 300 GHz WR-3 interface with dimensions of 0.864 × 0.432 mm$^2$ whose center aligns with that of the coupling slot.

Dimensions of the antenna are illustrated in Fig. 2(d). The dimension of the radiating window can be set freely as long as it can accommodate the four slots, and its upper opening has dimensions of 3 × 1.5 mm$^2$. The width of the center conductor is 0.3 mm, and the two center stubs are both 0.2 mm in length. The four slots share the same dimensions of 0.8 × 0.3 mm$^2$, and the slot spacing is 0.5 mm, i.e., half free-space wavelength at 300 GHz. The upper opening of the air space and coupling slot have the dimensions of 2.3 × 0.9 mm$^2$ and 0.25 × 0.8 mm$^2$, respectively. It is worth mentioning that the antenna draw here is just the main body of the final realized full-scale antenna, which has extended areas containing eight holes reversed for locating pins and screws. All the dimensions are listed in Table I as well. The numerical results are obtained using the commercial software of high-frequency structure simulator (version 14) based on the finite-element method.

TABLE I
DETAILED DIMENSIONS OF THE PROPOSED ANTENNA (UNIT: mm)

| Parameter | $l_w$ | $w_w$ | $l_s$ | $w_s$ |
|---|---|---|---|---|
| Value | 3 | 1.5 | 0.8 | 0.3 |
| Parameter | $d_s$ | $l_b$ | $w_d$ | $\alpha$ |
| Value | 0.5 | 0.2 | 0.3 | 54.7° |
| Parameter | $l_a$ | $w_a$ | $l_c$ | $w_c$ |
| Value | 2.3 | 0.9 | 0.8 | 0.25 |
| Parameter | $t_1$ | $t_2$ | $t_3$ | $t_4$ |
| Value | 0.14 | 0.11 | 0.13 | 0.12 |

## B. Field Distributions

The magnitudes of the E-fields in the upper surface of the air space at 250, 275, 300, and 325 GHz are presented in Fig. 3(a). As seen, field modes at the four frequencies are similar, four half-period waves are distributed averagely and the electric maximum locates at the center of each slot. Fig. 3(b) shows the vector E-field distribution at the radiating surface. As seen, the vector E-fields within the four slots are all along the same direction, forming an in-phase radiating aperture in a wideband.

## C. Critical Parameter: Stub Length

The length of the blocking stub is a critical parameter influencing the impedance bandwidth. The impedance trajectories

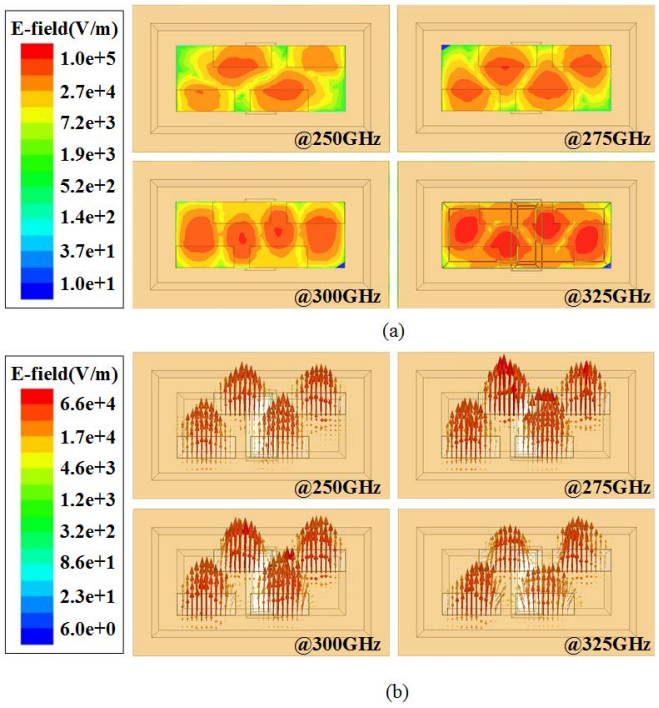


Fig. 3. (a) Magnitudes. (b) Vector E-field distributions at 250, 275, 300, and 325 GHz.

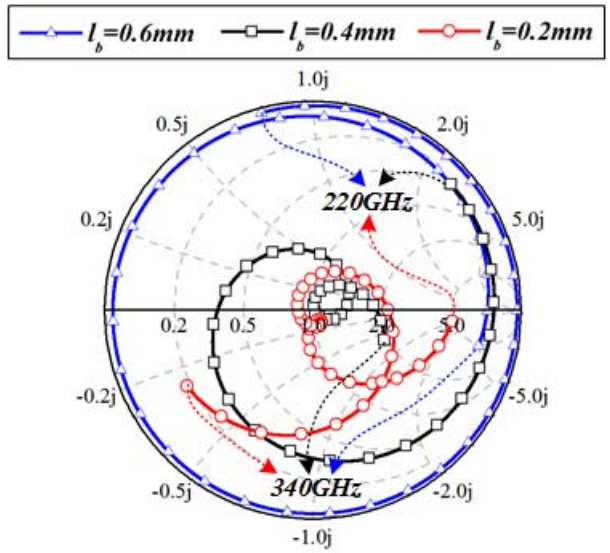


Fig. 4. Simulated impedance trajectories of different stub lengths.

on Smith chart within the frequency region 220–340 GHz under the stub lengths of 0.2, 0.4, and 0.6 mm are shown in Fig. 4. With the stub length decreasing, the impedance trajectory shrinks, indicating an enhanced bandwidth. This is caused by that the decreased stub length leads to an enlarged radiating aperture, making the antenna structure more open, resulting in a lower $Q$-factor. Here, a stub length of 0.2 mm, i.e., a slot length of 0.8 mm, is selected. Other antenna dimensions have been optimized to achieve the best antenna performance as well.

## IV. Hierarchical Silicon Bulk Micromachining

The fabrication processes used here include wet and dry etching and gold plating of the silicon bulk micromachining technology. The wet etching used here is anisotropic etching, based on that, the etching rates for different crystal's orientations are different, generating a concave cavity with four 54.7° slopes [45]. By controlling the etching time according to the etching speed and desired structure depth, the anisotropic wet etching that is fulfilled using the liquid of tetramethyl ammonium hydroxide ensures an etching precision of about 30 $\mu$m. The dry etching used here is through-wafer etching using sulfur hexafluoride gas that yields nearly plumb sidewalls with an etching precision as high as 4 $\mu$m.

The wet etching drives a single silicon layer to be divided into two sublayers for hierarchical micromachining. For the first layer, the radiating window was first made out using wet etching from the top, and then the four slots were produced using dry etching from the bottom. For the second layer, the air space and coupling slot were both processed out using wet etching from the top and bottom, respectively. The fabrication sequence of the two first sublayers matters, i.e., the wet etching (radiating window) goes first and then the dry etching (four slots), nevertheless, for the second two sublayers using both wet etching, the sequence does not matter. Through the parameter analysis, it is found that as long as the thickness of the radiating slots is less than 0.14 mm and the air space layer lies in 0.11–0.14 mm, the bandwidth achieves a good level and is rather robust to the fabrication tolerance. It is worth mentioning that the necessary condition for implementing hierarchical micromachining is that the wet etching process must be first used to manipulate one of the sublayers, and then the other can be disposed freely using any etching methods. Attributing to the hierarchical micromachining approach, to construct the proposed antenna, the required silicon substrate layers decrease by one compared to our previous design in [40]. When the four structures were made out, eight holes reserved for location pins and screws were fabricated using through-wafer dry etching.

After the etching processes were accomplished, all the faces and sidewalls of the two layers were electroplated with a 3.5 $\mu$m-thick gold layer with a tolerance of 0.5 $\mu$m. As a result, all the silicon substrates were covered by gold, generating a purely air-filled antenna without any silicon exposed outside, with the merit of low loss and high efficiency.

Finally, the two layers are assembled into a whole using the optical alignment and wafer bonding processes. The alignment process is accomplished using the optical alignment technology: with the help of a bonding machine; the two layers are aligned using a vision optical system and the alignment crosses of the two silicon layers. The alignment tolerance is better than 5 $\mu$m. The wafer bonding process is fulfilled as follows: clamp the two aligned layers with a special fixture and put them into the vacuum sintering furnace for baking under a controlled atmosphere for about 1 h. The clamp pressure and baking temperature gradually rise to their peaks, i.e., about 5 kN force and 350 °C with a duration time of about 10 min, and then the press and temperature return to zero force and

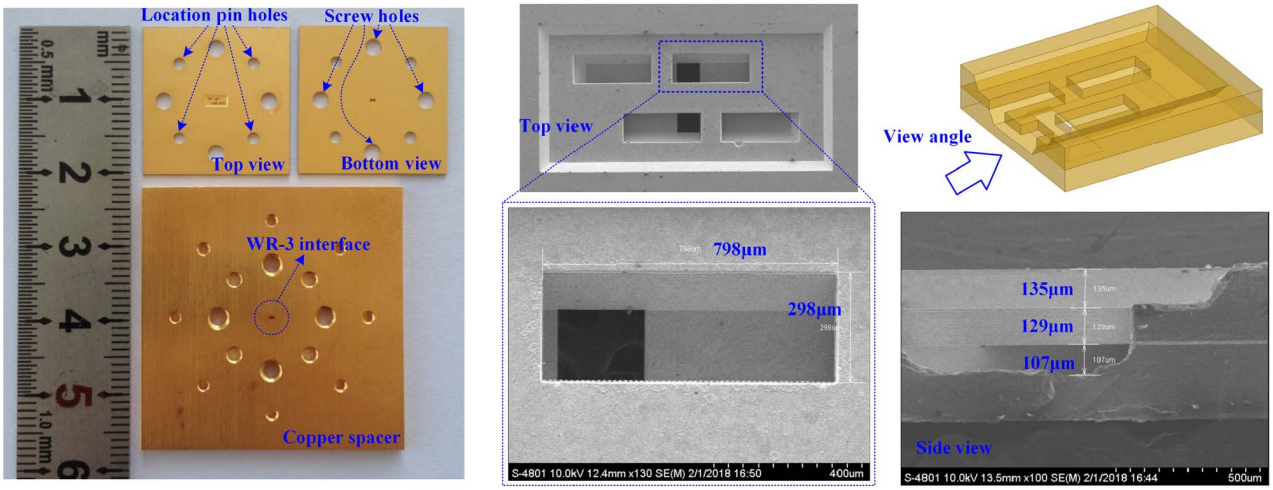


Fig. 5. (a) Fabricated prototypes of the proposed terahertz array and the copper spacer. (b) and (c) SEM photographs showing the top and side views.

room temperature. Finally, the adjacent gold-plated surfaces are melted and joined together.

## V. Experimental Result

The fabricated prototype is shown in Fig. 5(a), which shows the top and bottom views of the bonded antenna and the top view of a 2 mm-thick copper spacer. The two silicon layers and the copper spacer both have a square shape with side lengths of 20 and 35 mm, respectively. The copper spacer with a standard WR-3 waveguide inside has two functions: protecting the fragile silicon wafers and connecting the feeding waveguide and the proposed terahertz antenna. Finally, the proposed antenna, copper spacer, and a 300 GHz WR-3 waveguide are aligned and assembled together through the two location pins of the feeding waveguide and four extra screws. The SEM photographs and the realized dimensions are also shown. Fig. 5(b) shows the top view and the measured dimensions of the radiating slot. The measured length and width are, respectively, 798 and 298 $\mu$m, which are so close to the design values of 800 and 300 $\mu$m. This demonstrates that the precision of the dry etching is within 4 $\mu$m. Meanwhile, the edges of these structures are perfectly straight. Fig. 5(c) shows the side view (cutoff along one slot in $yz$ plane, see Fig. 5(b)) and the measured depths of the three etched sublayers. It is worth noting that the bulges and burrs are caused by incision. The measured depths of the three sublayers are, respectively, 135, 129, and 107 $\mu$m, which are also so close to the design values of 140, 110, and 130 $\mu$m. This demonstrates that the precision of the wet etching is within 30 $\mu$m. Clear tilted slopes caused by wet etching and nearly plumbed sidewalls caused by dry etching are observed, and the surface roughness looks smooth.

Reflection coefficient, gains, and radiation patterns were measured using a N5244A vector network analyzer and two frequency extenders with type WHMB-03-0002 FTL 10626. During the test, the source power was set to 0 dBm.

The simulated and measured magnitudes of the reflection coefficients are shown in Fig. 6(a), and they are in good

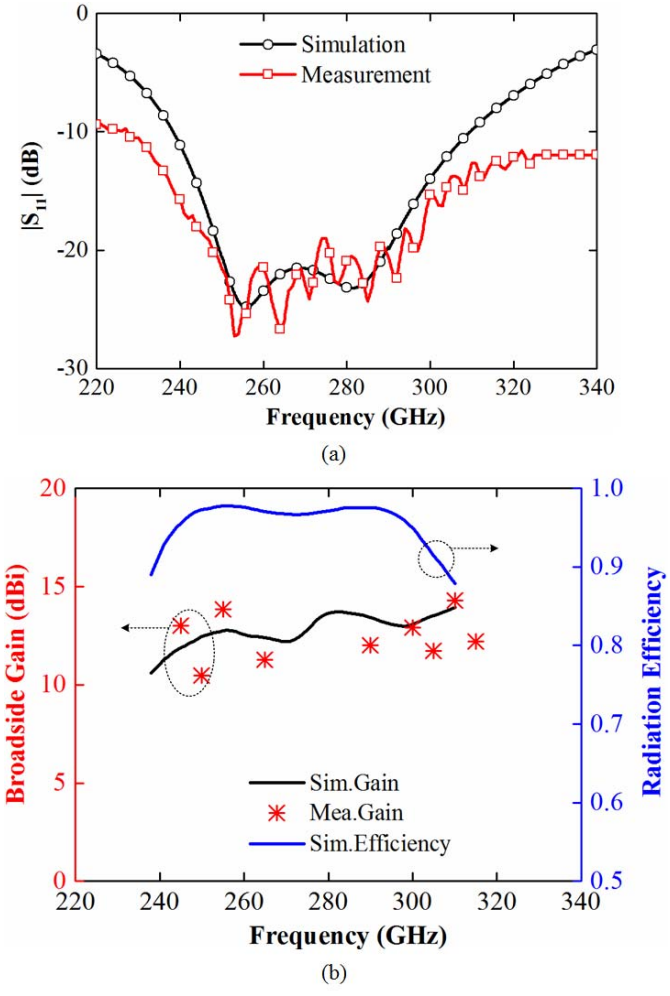


Fig. 6. (a) Simulated and measured $|S_{11}|$. (b) Simulated and measured broadside gains and simulated radiation efficiencies.

agreement. Restricted by the frequency extender, the available upper frequency limit is 340 GHz. The simulated bandwidth is 71.1 GHz from 238.4 to 309.5 GHz (25.95%), while the measured bandwidth is higher than 117.7 GHz from 222.3 to

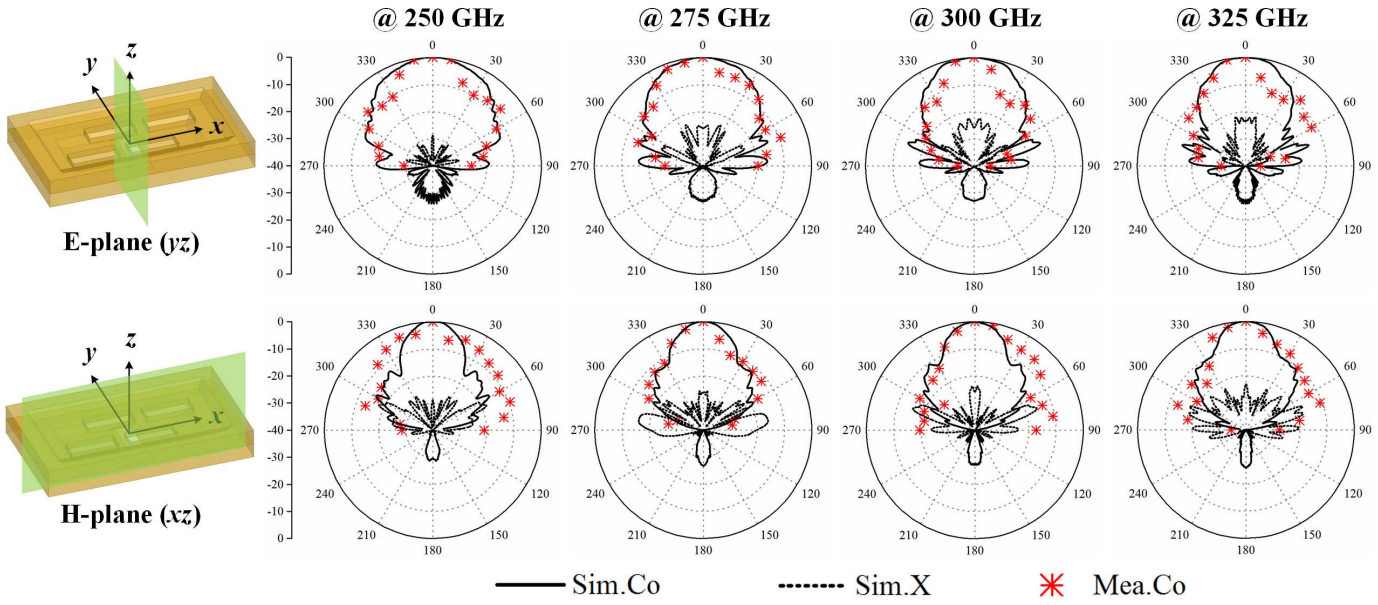


Fig. 7. Simulated normalized co-polarized and cross-polarized and measured co-polarized patterns in the two principal planes at 250, 275, 300, and 325 GHz.

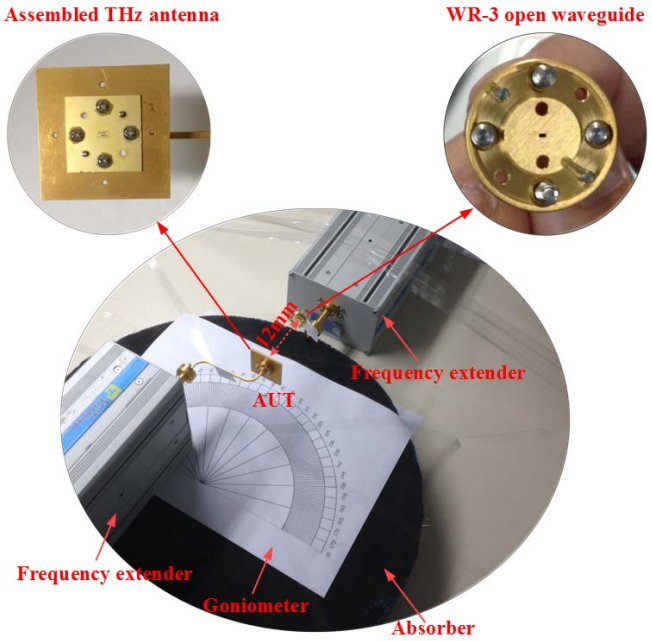


Fig. 8. Measurement setup.

above 340 GHz (>41.86%). The measured return loss and bandwidth are better than simulation because of the losses of the frequency extender and the transmission waveguide. A connection waveguide (as shown in Fig. 8 in this paper) is used to connect the frequency extender and the proposed antenna. The ripples in the measured $|S_{11}|$ are caused by the mismatches on the two ends of the connection waveguide.

The simulated broadside gains and radiation efficiencies are given in Fig. 6(b), exhibiting a high radiation performance: the gains and efficiencies are higher than 10.6 dBi and 87.9%, respectively, across the band. The measured broadside gains are also given. An average gain drop of 1.5 dB and the fluctuation are mainly because the receiving and gain calibration antennas are both electrically large WR-3 open waveguide that have a low-gain radiation pattern with many ripples.

The measured and simulated normalized radiation patterns in the two principal planes at 250, 275, 300, and 325 GHz are plotted in Fig. 7. The measured result only gives the co-polarized patterns in the upper half-space. As seen, stable simulated fan-shaped beams of good quality are observed across the frequency band. The measured patterns roughly agree with the simulated result in a certain degree. The discrepancies existing in the gains and patterns come from the test errors which are detailed as follows.

Fig. 8 shows the measurement setup. The proposed terahertz array acted as the transmitting antenna, and the standard WR-3 open waveguide acted as the receiving antenna and gain calibration antenna simultaneously. The distance between the antenna under test (AUT) and the receiver was 12 mm. A piece of wave absorber was placed underneath to create a stable test environment. The AUT was rotated manually with the help of a printed goniometer with a sampling interval angle of 10°, and only the radiation in upper half-space was measured. The test errors may include three aspects. First, the test environment was limited and unstable. The nearby EM environment was not friendly: the chassis on which the test system is located and the surfaces of the frequency extenders are both metallic boundaries, and the absorption rate of the available wave absorber at terahertz band is rather limited because the nominal upper frequency limit is only 40 GHz. Thus, these metallic surfaces may reflect and scatter the EM waves, deteriorating the measured result. On the other hand, several bulk and heavy equipment have occupied most of the space near the vector network analyzer, so the confined space limited accurate manual measurement, leading to increased test errors. Second, limited by the hardware equipment, the receiving

and calibration antennas used were the same WR-3 open waveguide. However, the open waveguide with dimensions of $0.864 \times 0.432$ mm$^2$ is fairly small compared with its flange with a diameter of 19 mm so the edge diffraction effect will produce lots of ripples in the radiation pattern. In addition to the abovementioned unstable test environment, the measured transmission coefficients were unsteady. This is the primary reason of the ups and downs in the measured gain curve and patterns. Third, when measuring the pattern, the alignment between the AUT and receiving antenna and rotation of the AUT were accomplished completely by sight with the help of the printed goniometer. It is difficult to obtain the accurate position just by visual inspection.

These errors are more like inevitable mistakes limited by the test equipment. If the proposed antenna is measured using a better test setup, such as perfect wave absorbers, more directive receiving and gain calibration horns, laser alignment instrument, and a mechanical rotary table, the acquired measured results should be far better and closer to the numerical ones.

As stated in [34], if the antenna input is changed from the waveguide interface to a ground–signal–ground input, the proposed air-filled terahertz antenna can be integrated with the other ICs within a single package, promoting the AiP solution.

## VI. Conclusion

In this paper, the first planar air-filled terahertz array is proposed and fabricated using the silicon bulk micromachining process. The proposed array is inspired by breaking the fringing field symmetry of the CCPW, and excellent performance is acquired. Different from the traditional silicon micromachining that manipulates the whole silicon wafer, the hierarchical micromachining approach enables a single silicon layer to be divided into two sublayers, leading to reduced antenna layers. On the other hand, the silicon substrates are fully covered with gold, and the EM wave encounters only air, forming a low-loss and high-efficiency terahertz antenna. The fabricated prototype shows that the measured result roughly agrees with the simulation. To the best of author's knowledge, this is the first time that a planar air-filled terahertz array is reported. Thanks to this fabrication process, antenna engineers can boldly design high-performance air-filled terahertz antennas using silicon substrate. Moreover, this silicon-based terahertz antenna can be integrated with other ICs, promoting the AiP solution.

## References


[1] P. H. Siegel, "Terahertz technology," *IEEE Trans. Microw. Theory Techn.*, vol. 50, no. 3, pp. 910–928, Mar. 2002.

[2] H.-J. Song and T. Nagatsuma, "Present and future of terahertz communications," *IEEE Trans. THz Sci. Technol.*, vol. 1, no. 1, pp. 256–263, Sep. 2011.

[3] H.-B. Liu, H. Zhong, N. Karpowicz, Y. Chen, and X.-C. Zhang, "Terahertz spectroscopy and imaging for defense and security applications," *Proc. IEEE*, vol. 95, no. 8, pp. 1514–1527, Aug. 2007.

[4] P. H. Siegel, "Terahertz technology in biology and medicine," *IEEE Trans. Microw. Theory Techn.*, vol. 52, no. 10, pp. 2438–2447, Oct. 2004.

[5] D. L. Woolard, R. Brown, M. Pepper, and M. Kemp, "Terahertz frequency sensing and imaging: A time of reckoning future applications?" *Proc. IEEE*, vol. 93, no. 10, pp. 1722–1743, Oct. 2005.

[6] T. Tajima, H.-J. Song, K. Ajito, M. Yaita, and N. Kukutsu, "300-GHz step-profiled corrugated horn antennas integrated in LTCC," *IEEE Trans. Antennas Propag.*, vol. 62, no. 11, pp. 5437–5444, Nov. 2014.

[7] J. Xu, Z. N. Chen, X. Qing, and W. Hong, "140-GHz planar broadband LTCC SIW slot antenna array," *IEEE Trans. Antennas Propag.*, vol. 60, no. 6, pp. 3025–3028, Jun. 2012.

[8] J. Xu, Z. N. Chen, and X. Qing, "270-GHz LTCC-integrated strip-loaded linearly polarized radial line slot array antenna," *IEEE Trans. Antennas Propag.*, vol. 61, no. 4, pp. 1794–1801, Apr. 2013.

[9] J.-H. Lee, N. Kidera, G. Dejean, S. Pinel, J. Laskar, and M. M. Tentzeris, "A V-band front-end with 3-D integrated cavity filters/duplexers and antenna in LTCC technologies," *IEEE Trans. Microw. Theory Techn.*, vol. 54, no. 7, pp. 2925–2936, Jul. 2006.

[10] Y. Li, Z. N. Chen, X. Qing, Z. Zhang, J. Xu, and Z. Feng, "Axial ratio bandwidth enhancement of 60-GHz substrate integrated waveguide-fed circularly polarized LTCC antenna array," *IEEE Trans. Antennas Propag.*, vol. 60, no. 10, pp. 4619–4626, Oct. 2012.

[11] G. T. A. Kovacs, I. N. Maluf, and K. E. Petersen, "Bulk micromachining of silicon," *Proc. IEEE*, vol. 86, no. 8, pp. 1536–1551, Aug. 1998.

[12] V. M. Lubecke, K. Mizuno, and G. M. Rebeiz, "Micromachining for terahertz applications," *IEEE Trans. Microw. Theory Techn.*, vol. 46, no. 11, pp. 1821–1831, Nov. 1998.

[13] M. O. S. Dantas, E. Galeazzo, H. E. M. Peres, and F. J. Ramirez-Fernandez, "Silicon micromechanical structures fabricated by electrochemical process," *IEEE Sensors J.*, vol. 3, no. 6, pp. 722–727, Dec. 2003.

[14] S. Darbari, S. Azimi, S. Mohajerzadeh, A. Sammak, N. Izadi, and S. Famini, "Hydrogenation-assisted lateral micromachining of (111) silicon wafers," *J. Microelectromech. Syst.*, vol. 17, no. 6, pp. 1489–1494, Dec. 2008.

[15] C. Jung *et al.*, "Silicon micromachining technology for THz applications," in *Proc. 35th Int. Conf. Infr. Millim. Terahertz Waves (IRMMW-THz)*, Rome, Italy, Sep. 2010, pp. 1–3.

[16] D. Xu, B. Xiong, G. Wu, Y. Wang, X. Sun, and Y. Wang, "Isotropic silicon etching with $XeF_2$ gas for wafer-level micromachining applications," *J. Microelectromech. Syst.*, vol. 21, no. 6, pp. 1436–1444, Dec. 2012.

[17] N. Llombart, G. Chattopadhyay, A. Skalare, and I. Mehdi, "Novel terahertz antenna based on a silicon lens fed by a leaky wave enhanced waveguide," *IEEE Trans. Antennas Propag.*, vol. 59, no. 6, pp. 2160–2168, Jun. 2011.

[18] N. Zhu and R. W. Ziolkowski, "Photoconductive THz antenna designs with high radiation efficiency, high directivity, and high aperture efficiency," *IEEE Trans. THz Sci. Technol.*, vol. 3, no. 6, pp. 721–730, Nov. 2013.

[19] A. Neto, N. Llombart, J. J. A. Baselmans, A. Baryshev, and S. J. C. Yates, "Demonstration of the leaky lens antenna at submillimeter wavelengths," *IEEE Trans. THz Sci. Technol.*, vol. 4, no. 1, pp. 26–32, Jan. 2014.

[20] A. A. Generalov, J. A. Haimakainen, D. V. Lioubtchenko, and A. V. Räisänen, "Wide band mm- and sub-mm-wave dielectric rod waveguide antenna," *IEEE Trans. THz Sci. Technol.*, vol. 4, no. 5, pp. 568–574, Sep. 2014.

[21] A. Rivera-Lavado *et al.*, "Dielectric rod waveguide antenna as THz emitter for photomixing devices," *IEEE Trans. Antennas Propag.*, vol. 63, no. 3, pp. 882–890, Mar. 2015.

[22] N. Ranjkesh, M. Basha, A. Taeb, and S. Safavi-Naeini, "Silicon-on-glass dielectric waveguide—Part II: For THz applications," *IEEE Trans. THz Sci. Technol.*, vol. 5, no. 2, pp. 280–287, Mar. 2015.

[23] N. Ranjkesh, A. Taeb, N. Ghafarian, S. Gigoyan, M. A. Basha, and S. Safavi-Naeini, "Millimeter-wave suspended silicon-on-glass tapered antenna with dual-mode operation," *IEEE Trans. Antennas Propag.*, vol. 63, no. 12, pp. 5363–5371, Dec. 2015.

[24] D. Hou, Y. Z. Xiong, W. L. Goh, S. Hu, W. Hong, and M. Madihian, "130-GHz on-chip meander slot antennas with stacked dielectric resonators in standard CMOS technology," *IEEE Trans. Antennas Propag.*, vol. 60, no. 9, pp. 4102–4109, Sep. 2012.

[25] Y. Liu *et al.*, "Millimeterwave and terahertz waveguide-fed circularly polarized antipodal curvedly tapered slot antennas," *IEEE Trans. Antennas Propag.*, vol. 64, no. 5, pp. 1607–1614, May 2016.

[26] C. Lee *et al.*, "Terahertz antenna arrays with silicon micromachined-based microlens antenna and corrugated horns," in *Proc. iWAT*, Seoul, South Korea, Mar. 2015, pp. 70–73.

[27] J. W. Britton *et al.*, "Corrugated silicon platelet feed horn array for CMB polarimetry at 150 GHz," *Proc. SPIE*, vol. 7741, Jul. 2010, pp. 247–258.

[28] Y. Liu, L.-M. Si, S.-H. Zhu, and H. Xin, "Experimental realisation of integrated THz electromagnetic crystals (EMXT) H-plane horn antenna," *Electron. Lett.*, vol. 47, no. 2, pp. 80–82, Jan. 2011.
[29] H.-T. Zhu, Q. Xue, J.-N. Hui, and S. W. Pang, "A 750–1000 GHz *H*-plane dielectric horn based on silicon technology," *IEEE Trans. Antennas Propag.*, vol. 64, no. 12, pp. 5074–5083, Dec. 2016.
[30] Y. Shang, H. Yu, H. Fu, and W. Lim, "A 239–281 GHz CMOS receiver with on-chip circular-polarized substrate integrated waveguide antenna for sub-terahertz imaging," *IEEE Trans. THz Sci. Technol.*, vol. 4, no. 6, pp. 686–695, Nov. 2014.
[31] W. H. Syed, G. Fiorentino, D. Cavallo, M. Spirito, P. M. Sarro, and A. Neto, "Design, fabrication, and measurements of a 0.3 THz on-chip double slot antenna enhanced by artificial dielectrics," *IEEE Trans. THz Sci. Technol.*, vol. 5, no. 2, pp. 288–298, Mar. 2015.
[32] X.-D. Deng, Y. Li, C. Liu, W. Wu, and Y.-Z. Xiong, "340 GHz on-chip 3-D antenna with 10 dBi gain and 80% radiation efficiency," *IEEE Trans. THz Sci. Technol.*, vol. 5, no. 4, pp. 619–627, Jul. 2015.
[33] S. Atakaramians, S. Afshar V. T. M. Monro, and D. Abbott, "Terahertz dielectric waveguides," *Adv. Opt. Photon.*, vol. 5, no. 2, pp. 169–215, Jun. 2013.
[34] P. L. Kirby, D. Pukala, H. Manohara, I. Mehdi, and J. Papapolymerou, "Characterization of micromachined silicon rectangular waveguide at 400 GHz," *IEEE Microw. Wireless Compon. Lett.*, vol. 16, no. 6, pp. 366–368, Jun. 2006.
[35] Y. Li, I. Mehdi, A. Maestrini, R. H. Lin, and J. Papapolymerou, "A broadband 900-GHz silicon micromachined two-anode frequency tripler," *IEEE Trans. Microw. Theory Techn.*, vol. 59, no. 6, pp. 1673–1681, Jun. 2011.
[36] C. A. Leal-Sevillano *et al.*, "Silicon micromachined canonical E-plane and H-plane bandpass filters at the terahertz band," *IEEE Microw. Wireless Compon. Lett.*, vol. 23, no. 6, pp. 288–290, Jun. 2013.
[37] T. J. Reck, C. Jung-Kubiak, J. Gill, and G. Chattopadhyay, "Measurement of silicon micromachined waveguide components at 500–750 GHz," *IEEE Trans. THz Sci. Technol.*, vol. 4, no. 1, pp. 33–38, Jan. 2014.
[38] T. Reck *et al.*, "A silicon micromachined eight-pixel transceiver array for submillimeter-wave radar," *IEEE Trans. THz Sci. Technol.*, vol. 5, no. 2, pp. 197–206, Mar. 2015.
[39] G. Chattopadhyay, T. Reck, C. Lee, and C. Jung-Kubiak, "Micromachined packaging for terahertz systems," *Proc. IEEE*, vol. 105, no. 6, pp. 1139–1150, Jun. 2017.
[40] L. Chang, Z. Zhang, Y. Li, S. Wang, and Z. Feng, "60-GHz air substrate leaky-wave antenna based on MEMS micromachining technology," *IEEE Trans. Compon., Packag. Manuf. Technol.*, vol. 6, no. 11, pp. 1656–1662, Nov. 2016.
[41] L. Chang, Z. Zhang, Y. Li, S. Wang, and Z. Feng, "Air-filled long slot leaky-wave antenna based on folded half-mode waveguide using silicon bulk micromachining technology for millimeter-wave band," *IEEE Trans. Antennas Propag.*, vol. 65, no. 7, pp. 3409–3418, Jul. 2017.
[42] L. Chang, Y. Li, Z. Zhang, X. Li, S. Wang, and Z. Feng, "Low-sidelobe air-filled slot array fabricated using silicon micromachining technology for millimeter-wave application," *IEEE Trans. Antennas Propag.*, vol. 65, no. 8, pp. 4067–4074, Aug. 2017.
[43] Y. Zhang and D. Liu, "Antenna-on-chip and antenna-in-package solutions to highly integrated millimeter-wave devices for wireless communications," *IEEE Trans. Antennas Propag.*, vol. 27, no. 10, pp. 2830–2841, Oct. 2009.
[44] R. N. Simons, *Coplanar Waveguide Circuits, Components, and Systems*, 2nd ed. New York, NY, USA: Wiley, 2004, pp. 107–108.
[45] V. K. Varadan, K. J. Vinoy, and K. A. Jose, *RF MEMS and Their Applications*, 2nd ed. New York, NY, USA: Wiley, 2003, chs. 1–8.

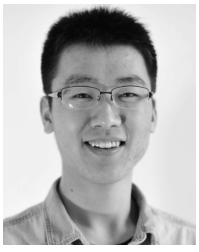

**Le Chang** (S'16) received the B.S. degree in electronics and information engineering from Xidian University, Xi'an, China, in 2012, and the Ph.D. degree in electrical engineering from Tsinghua University, Beijing, China, in 2017.

He is currently a Senior Engineer with Huawei Device Ltd., Beijing.

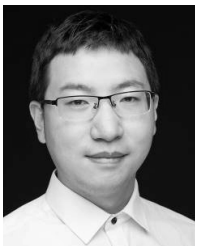

**Yue Li** (S'11–M'12–SM'17) received the B.S. degree in telecommunication engineering from Zhejiang University, Hangzhou, China, in 2007, and the Ph.D. degree in electronic engineering from Tsinghua University, Beijing, China, in 2012.

In 2010, he joined the Institute for Infocomm Research, A*STAR, Singapore, as a Visiting Scholar. In 2012, he joined the Hawaii Center of Advanced Communication, University of Hawaii at Mānoa, Honolulu, HI, USA. In 2012, he joined the Department of Electronic Engineering, Tsinghua University, as a Post-Doctoral Fellow. In 2013, he joined the Department of Electrical and Systems Engineering, University of Pennsylvania, Philadelphia, PA, USA, as Research Scholar. Since 2016, he has been with Tsinghua University, where he is currently an Assistant Professor. He is currently an Associate Professor with the Department of Electronic Engineering, Tsinghua University. He has authored or co-authored over 90 journal papers and 30 international conference papers. He holds 15 granted Chinese patents. His current research interests include metamaterials, plasmonics, electromagnetics, nanocircuits, mobile and handset antennas, MIMO and diversity antennas, and millimeter-wave antennas and arrays.

Dr. Li received the Issac Koga Gold Medal from URSI General Assembly in 2017, the Second Prize of Science and Technology Award of the China Institute of Communications in 2017, the Young Scientist Awards (four times) from the conferences of AT-RASC 2018, AP-RASC 2016, EMTS 2016, and URSI GASS 2014, the Best Paper Awards (seven times) from the conferences of CSQRWC 2018, NCMMW 2018 and 2017, APCAP 2017, NCANT 2017, ISAPE 2016, and ICMMT 2016, the Outstanding Doctoral Dissertation of Beijing Municipality in 2013, and the Principal Scholarship of Tsinghua University in 2011. He is serving as an Associate Editor of the IEEE TRANSACTIONS ON ANTENNAS AND PROPAGATION, the IEEE ANTENNAS AND WIRELESS PROPAGATION LETTERS, and Computer Applications in Engineering Education.

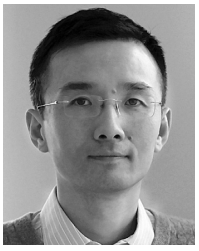

**Zhijun Zhang** (M'00–SM'04–F'15) received the B.S. and M.S. degrees from the University of Electronic Science and Technology of China, Chengdu, China, in 1992 and 1995, respectively, and the Ph.D. degree from Tsinghua University, Beijing, China, in 1999.

In 1999, he joined the Department of Electrical Engineering, University of Utah, Salt Lake City, UT, USA, as a Post-Doctoral Fellow, where he was appointed as a Research Assistant Professor in 2001. In 2002, he joined the University of Hawaii at Mānoa, Honolulu, HI, USA, as a Assistant Researcher. In 2002, he joined Amphenol T&M Antennas, Vernon Hills, IL, USA, as a Senior Staff Antenna Development Engineer and then promoted to Antenna Engineer Manager. In 2004, he joined Nokia Inc., San Diego, CA, USA, as a Senior Antenna Design Engineer. In 2006, he joined Apple Inc., Cupertino, CA, USA, as a Senior Antenna Design Engineer and then promoted to Principal Antenna Engineer. Since 2007, he has been with Tsinghua University, where he is currently a Professor with the Department of Electronic Engineering. He has authored *Antenna Design for Mobile Devices* (Wiley, 2011).

Dr. Zhang served as an Associate Editor of the IEEE TRANSACTIONS ON ANTENNAS AND PROPAGATION from 2010 to 2014 and the IEEE ANTENNAS AND WIRELESS PROPAGATION LETTERS from 2009 to 2015.

**Shaodong Wang**, photograph and biography not available at the time of publication.

**Zhenghe Feng** (M'05–SM'08–F'12) received the B.S. degree in radio and electronics from Tsinghua University, Beijing, China, in 1970.

Since 1970, he has been an Assistant, a Lecture, an Associate Professor, and a Full Professor with Tsinghua University. His current research interests include numerical techniques and computational electromagnetics, RF and microwave circuits and antennas, wireless communications, smart antenna, and spatial-temporal signal processing.